Journal of Micromechanics and Microengineering

PAPER

Compression and decompression of structural tantalum films exposed to buffered hydrofluoric acid

To cite this article: Longchang Ni *et al* 2020 *J. Micromech. Microeng.* **30** 055011

IOP Publishing Journal of Micromechanics and Microengineering
J. Micromech. Microeng. **30** (2020) 055011 (9pp) https://doi.org/10.1088/1361-6439/ab7c35

Compression and decompression of structural tantalum films exposed to buffered hydrofluoric acid

Longchang Ni[1], Burcu Karagoz[2], Andrew J Gellman[2,3] and Maarten P De Boer[1]

[1] Department of Mechanical Engineering, Carnegie Mellon University, Pittsburgh, PA 15213, United States of America
[2] Department of Chemical Engineering, Carnegie Mellon University, Pittsburgh, PA 15213, United States of America
[3] Wilton E. Scott Institute for Energy Innovation, Carnegie Mellon University, Pittsburgh, PA 15213, United States of America

E-mail: mpdebo@andrew.cmu.edu

Received 19 December 2019, revised 14 February 2020
Accepted for publication 3 March 2020
Published 22 April 2020

Abstract

As a refractory metal with a high melting temperature and large coefficient of thermal expansion, tantalum (Ta) is of great interest as a structural material in MEMS. One of the major issues with any freestanding structure, however, is the control of residual stress. Here, we observe that suspended fixed–fixed beams made from Ta films under tension buckle after a buffered hydrofluoric (BHF) acid release step, implying a large change of stress towards compression. We find that the change in uniaxial stress is proportional to BHF exposure time and reaches −1 GPa after 150 min. Although there are many sources of residual stress in metal thin films, we demonstrate definitively that hydrogen (H) injection due to BHF is the major cause of this change. We show further that the residual stress can be largely recovered by degassing at 500 °C in a high vacuum environment.

Keywords: tantalum thin films, compressive stress, buffered hydrofluoric acid, hydrogen injection, degas

(Some figures may appear in colour only in the online journal)

1. Introduction

Tantalum (Ta) is of interest as a structural material in MEMS due to its unique combination of characteristics including high melting temperature ($T_m = 3017$ °C), high coefficient of thermal expansion (CTE), a passive protective oxide film, and good mechanical properties. For example, in a biomimetical cochlear implant application [1], Ta fixed–fixed beams served as resonant gates. There, Ta was chosen because it has a relatively low ratio of Young's modulus E to density ρ ($E/\rho = 10.7$ MPa/(kg m^{-3})), which is 40% that of aluminum (26 MPa/(kg m^{-3})). Ta has also been investigated in radio frequency switches due to its high creep resistance [2]. Due to Ta's high bulk CTE, 6.3 $\mu\epsilon$/°C [3] compared to that of a silicon substrate (2.7 $\mu\epsilon$/°C [4]), Ta thermal actuators could operate as passive thermal switches, similar to [5].

However, in MEMS applications, low residual stress is often needed to achieve the required function and residual stress control is required to accurately predict device performance. For instance, a low average stress and stress gradient are desirable for RF switches [2]. Residual stress also affects the dynamic response of Ta clamped–clamped beam structures [6]. But stress control is a complex issue in metal thin films, where residual stresses are strongly dependent on deposition conditions and on subsequent thermal treatments [7–10].

Of particular interest in this work, a large shift, not precisely quantified but on the order of hundreds of MPa, in Ta fixed–fixed beams towards more compressive stress was measured by Al-masha'al *et al* after two different release processes [6, 11]. In the first process, the sacrificial layer was a photoresist, and the release process was an oxygen plasma ash. In the second process, the sacrificial layer was silicon oxide, and the

release process was a buffered hydrofluoric (BHF) acid etch. To be able to use Ta in MEMS, the underlying mechanism responsible for this stress change must be clarified, and methods to prevent or reverse it must be found. Here, by detecting species outgassing from BHF-treated Ta films using a quadrupole mass spectrometer, we determine unambiguously that the compressive residual stress after a BHF etch arises from atomic hydrogen incorporation into the Ta film from the weak acid. We also demonstrate that hydrogen can be removed by a degassing procedure, and that the original residual stress can largely be recovered.

Although we study Ta here, this work is of general interest. The ability to absorb hydrogen is common to many metals [12, 13]. Absorbed hydrogen atoms occupy interstitial sites in the host-metal crystal lattice and in most cases have a deleterious influence. In bulk or thin film studies outside the context of MEMS, it has been observed that material properties and parameters such as residual stress [14, 15], lattice constant [16–18], resistivity [19], interfacial adhesion [20] or delamination [21–23], embrittlement [24], and plastic deformation [25] are all affected by H. In MEMS, exposure to BHF will likely remove a passive oxide film that often otherwise serves as a barrier to hydrogen incorporation [26]. As BHF is widely used in micro- and nanofabrication, any metallic film can potentially be affected. Therefore, the Ta/BHF interaction serves as a model system that can lend insight to a wide range of materials and the associated issues arising from hydrogen incorporation.

2. Experiment

2.1. Specimen preparation and characterization

The substrates used are $4''$ (100) Si wafers with 1 μm thick thermally grown oxide. Ta films are sputtered onto the substrate to a nominal thickness of $h_f = 2.5\mu$m, a typical thickness for surface micromachining structural materials, in a load-locked DC magnetron sputtering system (CVC Connexion Cluster Tool) at a base pressure lower than 7×10^{-8} Torr without intentional heating or biasing. At a power of 250 W, the deposition rate is approximately 19 nm min^{-1} using this standard recipe in our fabrication facility. Sputter deposition of a 45 nm thick Cr follows, which serves as the hard mask for Ta etch. The Cr mask is patterned using photolithography and ion milling. The Ta film is then reactively ion etched (RIE'd). At this point, the cross-section is schematically represented in figure 1(a). Next, the Cr hard mask is stripped. Then the sacrificial oxide is removed at room temperature by BHF (5 parts 40% NH_4F:1 part 49% HF). Finally, critical point drying renders the structures freestanding (figure 1(b)). The fabricated fixed–fixed beams have widths of 10 or 20 μm and lengths of 100, 250, 500, 750 or 1000 μm.

The change in curvature due to the Ta deposition of each wafer is conveniently measured during the process flow using a Tencor Flexus tool (FLX-2320), and the biaxial residual stress σ_f^b is characterized by applying the Stoney equation [27]

$$\sigma_f^b = \frac{E_s h_s^2}{6(1-\nu_s)h_f}\left(\frac{1}{R}-\frac{1}{R_0}\right) \tag{1}$$

where E_s, ν_s, and h_s are the Young's modulus, Poisson's ratio and thickness of the substrate, respectively, and R_0 and R are the radii of curvature before and after thin film deposition, respectively. Crystal structures are determined on separately-deposited blanket wafers using x-ray diffraction (XRD) under conventional reflective configurations, with a copper anode operated at 45 kV and 40 mA (Philips X'pert Pro MRD, model no. PW3040/60). The Young's modulus of the blanket Ta films is found from nanoindentation [28]. Fixed–fixed beam deflections are determined by interferometry. Resistivity is measured using a standard four-point probe configuration.

2.2. Buckling analysis

Once released, fixed–fixed beams under sufficiently high compression will buckle to partially relieve their residual stress. The critical uniaxial buckling stress for fixed–fixed boundary conditions is [29, 30]

$$\sigma_{cr}^u = \frac{\pi^2}{3}E_f\left(\frac{h_f}{L}\right)^2 \tag{2}$$

where L is the length of the beam and E_f is the film's Young's modulus. The buckle amplitude A is sensitive to the compressive stress, and the uniaxial residual stress σ_b^u of fixed–fixed beams before buckling can be determined by [29]

$$\sigma_b^u = -\frac{\pi^2 E_f}{L^2}\left(\frac{A^2}{4}+\frac{h_f^2}{3}\right) \tag{3}$$

The shape of buckle profile is sinusoidal according to [29]

$$w(x) = \frac{A}{2}\left(1+\cos\frac{2\pi x}{L}\right), -\frac{L}{2} \le x \le \frac{L}{2} \tag{4}$$

where $w(x)$ is the deflection and x is the position along the beam.

Fixed–fixed beams with lengths L = 250, 500, 750 and 1000 μm are used for stress extraction. Using equation (2), σ_{cr}^u stresses are calculated to be −59.9 MPa, −15.0 MPa, −6.7 MPa, and −3.7 MPa, respectively. In this work, because the uniaxial residual stress of compressively-stressed blanket β-Ta films is −92.0 MPa (extracted using equation (1) and equation (5), as shown in section 3), beams of these lengths are all expected to buckle. At this residual stress level, the critical buckling length is $L_{cr} \approx 200$ μm (equation (2)). Equation (3) is accurate as long as beams have lengths greater than $1.1L_{cr}$ [29]. Therefore, all the measured beams are expected to provide accurate results.

Consideration of the derivation of the Stoney equation (1) leads to the conclusion that it measures the average residual stress and is insensitive to the stress gradient. Likewise, rigid support posts cancel stress gradient effects in buckled fixed–fixed beams. Because the support posts in this work are relatively stiff while the measured beams are significantly longer

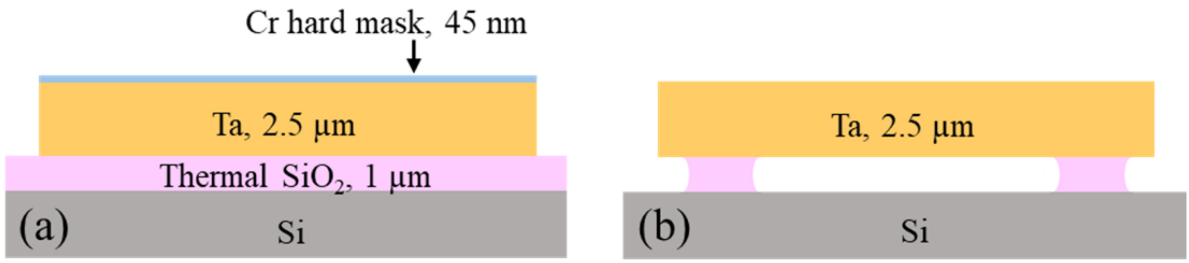

Figure 1. Fabrication process flow of fixed–fixed beams. (a) After Ta RIE. (b) After Cr mask strip and structure release.

than $1.1L_{cr}$, the equation (3) values are also insensitive to residual stress gradient. However, it should be noted that specimens measured using equation (1) reflect an average across the wafer, while those measured using equation (3) represent local values. Given that the sputter target is $12''$ while the wafers measured are $4''$, it is expected that the thickness and stress uniformity across the wafers is high.

2.3. Degassing

A UHV chamber is used to measure H_2 degassing with mass spectrometry. The system base pressure is 1×10^{-8} Torr, while the operating pressure below 1×10^{-7} Torr. A 1×1 cm^2 piece is cleaved from a blanket Ta wafer and serves as the specimen. It can be heated and actively cooled in the temperature range 100–900 K by resistive heating and liquid N_2 cooling. The temperature is measured using $0.01''$ K-type thermocouples. The specimens are heated from 300 K to 873 K at 0.25 K s^{-1} while H_2 desorption is recorded by a Dycor quadrupole mass spectrometer (MA200MFG).

Degassing of fixed–fixed beams is performed in a Kurt J. Lesker sputter system (Model # PVD75) at 500 °C. The system base pressure is 5×10^{-8} Torr. The pressure at 500 °C is 1.9×10^{-7} Torr.

3. Results and discussion

3.1. β-Ta films are used to show that hydrogen is responsible for a large residual stress change

Ta films with various initial residual stresses, spanning both tension and compression, are deposited by varying the Ar pressure. This is a well-known technique to adjust σ_R^b of sputter-deposited films as the sputter pressure can change the energetic particle bombardment intensity [31]. After release, fixed–fixed beams made from Ta films originally under compressive stress buckle, as expected because the compressive stress is beyond σ_{cr}. However, similar to Al-Masha'al *et al* [11], it is found that beams made from *tensile-stressed* films also buckle. Figure 2 shows buckled beams that were deposited under a moderate tensile stress of 21 MPa. Therefore, the residual stress changes during the fabrication process.

Given the fabrication process flow as shown in figure 1, we assume the stress change takes place either during dry etch of the Ta films or structure release. It is known that in a typical RIE, ion bombardment is an important physical process that removes etch inhibitors and enhances the etch rate. It is shown in [32] that Ta films exposed to ion bombardment can exhibit a stress change towards compression. The stress change depends on the bombardment intensity, and a large change of approximately up to −3 GPa was reported [32]. To test whether ion bombardment affects the residual stress here, the same RIE process is conducted on a 2.5 μm thick blanket Ta film covered by a 45 nm thick Cr. This mimics the environment that the unetched Ta areas experience. The change in σ_R^b of the blanket film, from +60 MPa to +56 MPa before and after RIE, respectively, is negligible. This is likely because the bombardment only affects near-surface atoms, which is significant for the 50 nm thick film reported in [32], but negligible for the much thicker film in this work.

The above result leads us to suspect that the stress change is caused by the release process. However, BHF is usually considered compatible with the Ta metal as it is much less aggressive than concentrated HF and the etch rate of Ta in BHF is known to be slow or zero [33]. But it is also known that Ta can absorb a significant amount of hydrogen (over 40 atomic % H in Ta at room temperature in an H_2 pressure of 1×10^{-5} Torr [34]), and a limiting composition is $TaH_{1.0}$ [35]. Known routes to introduce hydrogen into Ta include exposure to H_2 gas environment [17, 18, 25, 34, 36, 37], electrochemical charging [14–17, 22, 25, 38–41] and H_2 plasma [23]. If Ta does absorb hydrogen during BHF release, a compressive stress can be expected due to constrained lattice expansion.

To investigate whether hydrogen is absorbed during the release process, we expose blanket Ta films to BHF for increasing times and measure σ_f^b before and after BHF treatment. The uniaxial stress,

$$\sigma_f^u = \sigma_f^b (1 - \nu_f), \tag{5}$$

where ν_f is film Poisson's ratio, of 6 wafers exposed to BHF for 10, 35, 60, 90, 120 and 150 min, is calculated. Based on 24 nanoindentation measurements, the Young's modulus in the as-deposited condition is 181 ± 1.3 GPa. After 150 min exposure to BHF the same modulus was measured. The stress change increases almost linearly with BHF treatment time, and the stress increases towards compression up to 490 MPa after 150 min. The results are plotted in figure 3(a) (blanket β-Ta film, red), where a negative stress change means an increase in the compressive stress.

Similarly, longer immersion in BHF also results in a higher compressive stress in fixed–fixed beams. However, for the

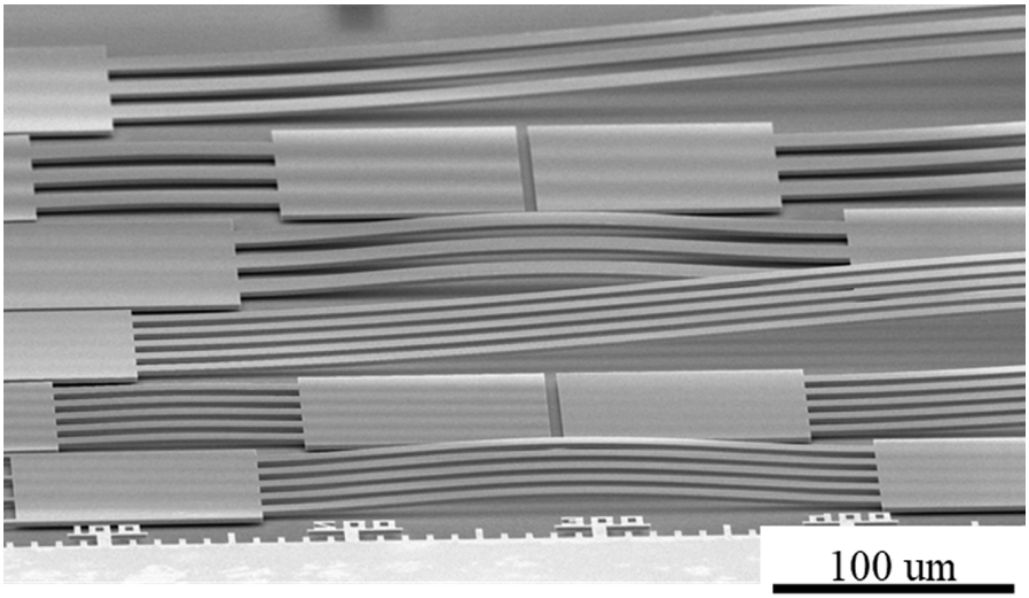

Figure 2. β-Ta fixed–fixed beams that were deposited under tension buckled after fabrication (the contrast on pads is an SEM artifact).

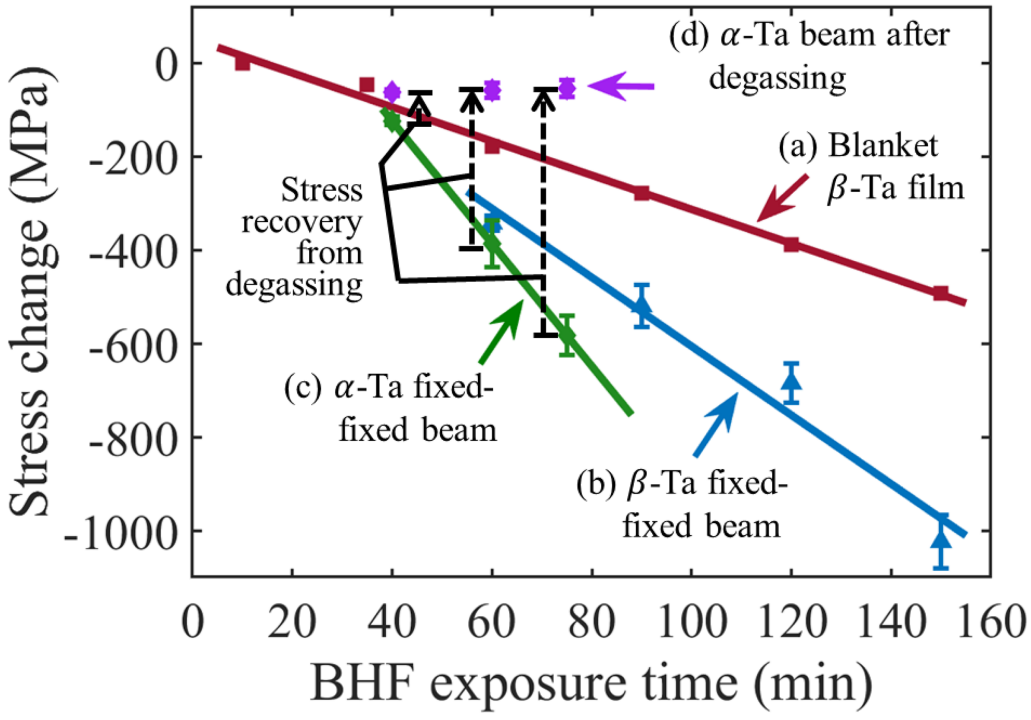

Figure 3. Stress change of blanket Ta films and fixed–fixed beams as a function of BHF exposure time. (a) Blanket β-Ta film, (b) β-Ta fixed–fixed beam, (c) α-Ta fixed–fixed beam, (d) α-Ta beam after degassing. Vertical dashed arrows denote residual stress recovery due to degassing. Note: the biaxial stress of blanket films is extracted using Stoney equation (1), which is then converted to uniaxial stress using equation (5). The uniaxial stress of fixed–fixed beams is extracted using equation (3).

same amount of time, BHF has a larger effect on beam structures than blanket films, which will be explained later. The uniaxial stress variation of fixed–fixed beams (β-Ta fixed–fixed beams, blue) is also shown in figure 3(b), where the range indicates one standard deviation as measured from ten beams. The 10 min and 35 min data are absent as the beams are not released. Figure 3 summarizes the most important results of this work and will be expanded upon below.

We present an example of the fixed–fixed beam stress change extraction. The buckle amplitude of an $L = 500$ μm beam after 60 min BOE exposure is measured as 15.31 μm. Using $h_f = 2.5$ μm, equation (3) gives a uniaxial residual stress

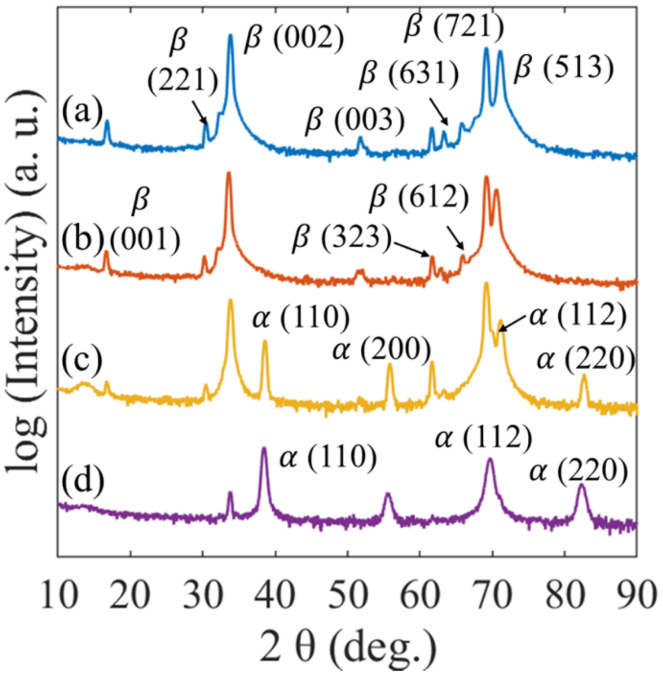

Figure 4. XRD diagrams of (a) as-deposited β-Ta films, (b) β-Ta films after 2.5 h BOE exposure, (c) β-Ta films after anneal at 500 °C for 20 min and (d) as-deposited α-Ta films on a Cr seed layer.

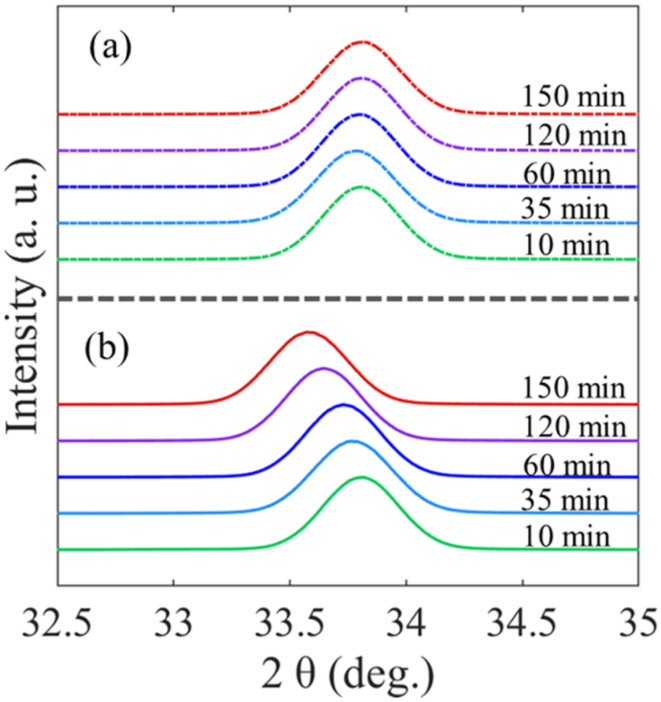

Figure 5. XRD diagrams of (002) plane (a) before and (b) after 10–150 min BOE exposure. This experiment was carried out on five individual wafers.

of −434 MPa. Before the beam fabrication process, the biaxial residual stress of the as-deposited blanket β-Ta film is extracted to be −139 MPa using the Stoney equation (1), which corresponds to a uniaxial residual stress of −92.0 MPa using equation (5). Therefore, the uniaxial residual stress change after BOE exposure is −342 MPa.

X-ray diffraction of an as-deposited blanket Ta film indicates the metastable β-phase, which has a tetragonal unit cell [42–44]. A resistivity of 172 $\mu\Omega$ cm is measured, also in good agreement with the known relatively high resistivity of 170–210 $\mu\Omega$ cm for β-Ta [44]. A 2.5 h BHF treatment does not lead to a phase transition or a change in texture. This observation is made by comparing figures 4(b) and (a).

However, the diffraction peaks move towards smaller diffraction angles with increasing BHF exposure. This lends support to the idea that hydrogen has been incorporated, as it expands the crystal lattice and increases the out-of-plane lattice constant. Comparison of high angular resolution plots of the (002) plane for five specimens before and after 10 to 150 min BHF exposure clearly shows that the diffraction angle θ becomes smaller and that the shift increases with exposure time, as seen in figure 5.

To conclusively demonstrate that hydrogen is injected into the Ta film during BHF exposure, degassing is performed on a blanket film submersed in BHF for 2 h. Another specimen without BHF exposure is also analyzed. H_2 desorption from the acid-treated specimen begins at 400 °C, reaches a maximum at 500 °C and becomes negligible at 570 °C, as indicated by the black line in figure 6. The BHF-treated specimen is reheated to check whether there residual H_2 remains. The minimal amount of H_2 desorption reveals that little further H_2 desorbed during the second thermal cycle (figure 6, red line). The rate of H_2 degassing for the specimen not exposed to BHF (figure 6, blue line) at 400 °C is 300 times less than the maximum rate for the specimen exposed to BHF, which occurs at 500 °C. The integrated amount over the temperature range from 27 °C to 600 °C of H_2 degassing from the specimen without BHF treatment is 1.4% of the amount from the BHF-treated specimen.

Table 1. Curve fitting of figure 3 stress change as a function of BHF exposure time.

(a) Blanket β-Ta film	$\Delta\sigma_R = -3.64t + 51.16$
(b) β-Ta fixed–fixed beam	$\Delta\sigma_R = -7.35t + 130.00$
(c) α-Ta fixed–fixed beam	$\Delta\sigma_R = -13.07t + 398.40$

Figure 6 confirms that the compressive residual stress arises from hydrogen absorption during BHF treatment. This also explains why BHF influences the stress of fixed–fixed beams more than that of blanket films. Namely, while hydrogen atoms can diffuse into blanket films only through the top surface, they can diffuse into fixed–fixed beams through the bottom surface as well as through their side walls. Therefore, fixed–fixed beams develop a higher compressive stress than blanket films for a given amount of time, while longer BHF exposure enlarges this difference. This is seen by comparing the stress changes of β-Ta fixed–fixed beams (blue curve, figure 3(a) to blanket films (red curve, figure 3(b) as a function of BHF exposure time. We observe that the slope of the former is almost twice that of the latter, as quantified in rows (a) and (b) of table 1. This also indicates that fixed–fixed beams absorb approximately twice as much as hydrogen as blanket films.

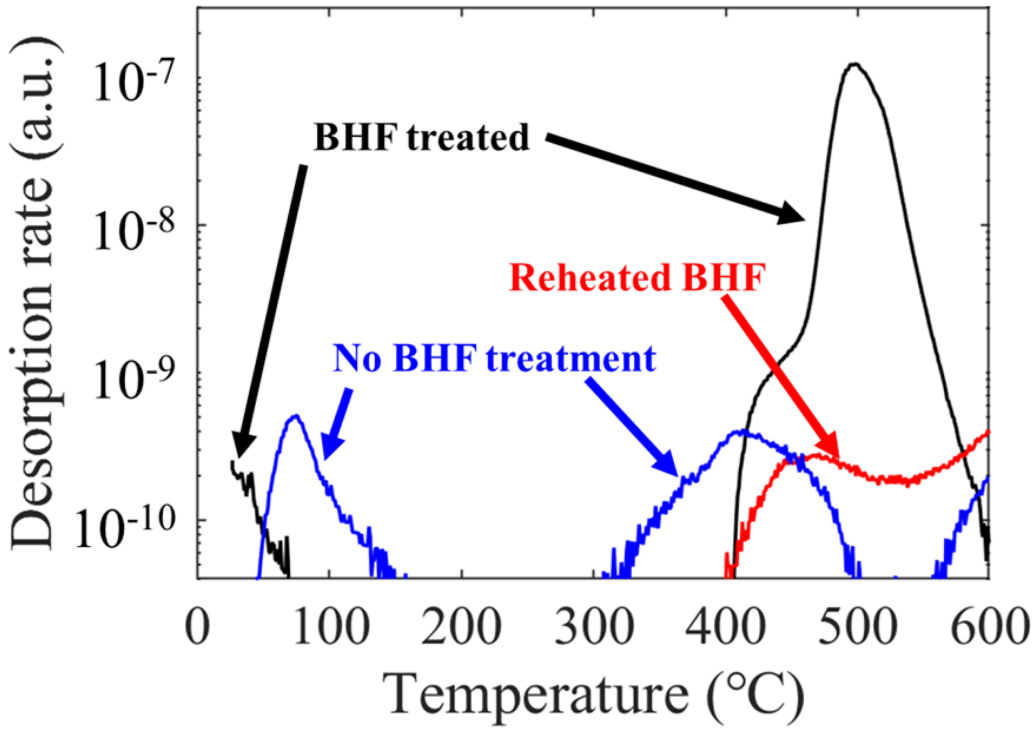

Figure 6. H_2 desorption rate from Ta thin film heated at 0.25 °C s^{-1}. The threshold for significant rate is set at $4{\cdot}10^{-11}$.

As hydrogen has been identified as the origin of stress shift towards compression, one interesting topic is its distribution through the film thickness. It is likely that the hydrogen concentration is rather uniform as the diffusion coefficient of hydrogen in Ta is on the order of $D_H^{Ta} = 10^{-6}\,\mathrm{cm^2\,s^{-1}}$ at room temperature [37], which means that hydrogen diffuses through the film thickness in $(h_f)^2/D_H^{Ta} \approx 0.06$ s. However, defects such as grain boundaries, dislocations and vacancies can be trap sites for hydrogen atoms, which can therefore change the local hydrogen affinity and concentration [45]. A detailed experimental measurement of the hydrogen profile would be an interesting subject for future work.

Our data suggests that the shift to compressive stress in Ta measured by Al-masha'al *et al* [11] when using a PECVD SiO_2 sacrificial layer and a BHF release results from hydrogen injection by the acid. In their other release process, the authors use 8 μm of a polyimide sacrificial layer and oxygen plasma ashing and also reported a large shift towards compressive stress [11]. We hypothesize that this is due to one of two effects. First, the oxygen plasma may release hydrogen atoms in the thick polyimide, which is subsequently absorbed by Ta films. Second, oxygen from the plasma diffusing into the film is known to generate compressive stress [46].

3.2. α-Ta films are used to show that the hydrogen effect is largely reversible

Thus far, the work we report has been conducted on β-Ta films. If the film deforms only elastically during hydrogen absorption, the residual stress should be recovered after degassing. However, a confounding factor is that the metastable β-Ta transforms to the stable α-phase with a BCC unit cell starting at temperatures as low as 300 °C. This transformation completely relaxes the intrinsic compressive stress and eventually results in a tensile stress [47, 48]. Knepper *et al* [48] attributed the increase in tensile stress to film densification due to differences in the β- and α-phase densities and to grain growth. The XRD diagram of β-Ta films after annealing at 500 °C for 20 min, confirms that the β-Ta partially transforms to the α phase, as seen in figure 4(c). As shown in figure 6, hydrogen desorption begins just above 400 °C and peaks at 500 °C, so the phase transition makes it impossible to independently isolate the effect of hydrogen degassing on residual stress.

Although sputter-deposited Ta films usually assume the tetragonal β-phase [42], they can nucleate and grow in the α-phase on certain seed layers [44, 47, 49–51]. We choose a 10-nm thick Cr seed layer to produce α-Ta. The unit cell of as-deposited α-Ta seeded by Cr is confirmed by XRD, as shown in figure 4(d). In this way, the stress change induced by the phase transition can be avoided. To stabilize the microstructure and avoid any stress evolution due to thermal treatment during degassing, the blanket α-Ta film is next annealed at 600 °C for 30 min. The biaxial residual stress is −358 MPa after anneal. A residual stress near 0 MPa is achievable in principle by adjusting the sputter pressure, but stress optimization has not yet been conducted.

Following a similar process flow to figure 1, fixed–fixed beams made from α-Ta are fabricated and released in BHF for 40 min, 60 min and 75 min (a longer exposure than 75 min to BHF leads to beam delamination of α-Ta). The stress change, $\Delta\sigma_R^u$, after release of α-Ta beams is determined from the effective uniaxial stress in the blanket film. It is higher than that

of β-Ta, as plotted by the green line, figure 3(c). This is likely because the more closely packed crystal structure of α-Ta [48] is more sensitive to hydrogen incorporation. The curve fitting for α-Ta fixed–fixed beams is also shown in table 1. Degassing is performed at 500 °C for 20 min, and $\Delta\sigma_R^b$ is also plotted as indicated by the purple points in figure 3(c) (green line). The final change in stress is below −60 MPa after degassing, indicating that the residual stress is largely recovered, as indicated by the vertical dashed black arrows in figure 3.

It was shown in [52] that above 375 °C, interstitial oxygen from a Ta_2O_5 surface layer diffuses into Ta. In [48], it was observed that native Ta_2O_5 increases the compressive stress upon annealing at 375 °C. Therefore, a possible reason for the remaining stress is that oxygen in the thin (∼2 nm) tantalum oxide layer that forms in air on the surface of fixed–fixed beams after release diffuses interstitially into the beams during degassing. Alternatively, a minimal amount of deeply-trapped residual hydrogen remains due to the high affinity of Ta to hydrogen [35]. A third possibility is that the remaining stress is actually due to residual deformations induced by residual plasticity in regions of high local strain and high hydrogen concentration. However, beams of different lengths recover the same amount of stress. Therefore, this possibility seems unlikely.

To show the direct effect of hydrogen degassing on α-Ta fixed–fixed beam deflections, representative interferograms were taken. Comparison of a buckled beam after 1 h BHF release and after hydrogen desorption indicates fewer fringes and a lower buckle amplitude after degassing, corresponding to a relaxation of compressive stress to a level nearly commensurate with the as-deposited blanket wafer. This is seen by comparing figures 7(a) and (b), and the associated beam deflection curves are seen in figure 7(c).

At 500 °C, this degassing temperature is relatively low compared to 1000 °C which is typically used to anneal stress in polycrystalline silicon MEMS [53]. With careful attention to initial deposition stress of α-Ta films and subsequent degassing under high vacuum, it should be possible to achieve low residual stress Ta films. The results may apply to other metals that are exposed to BHF.

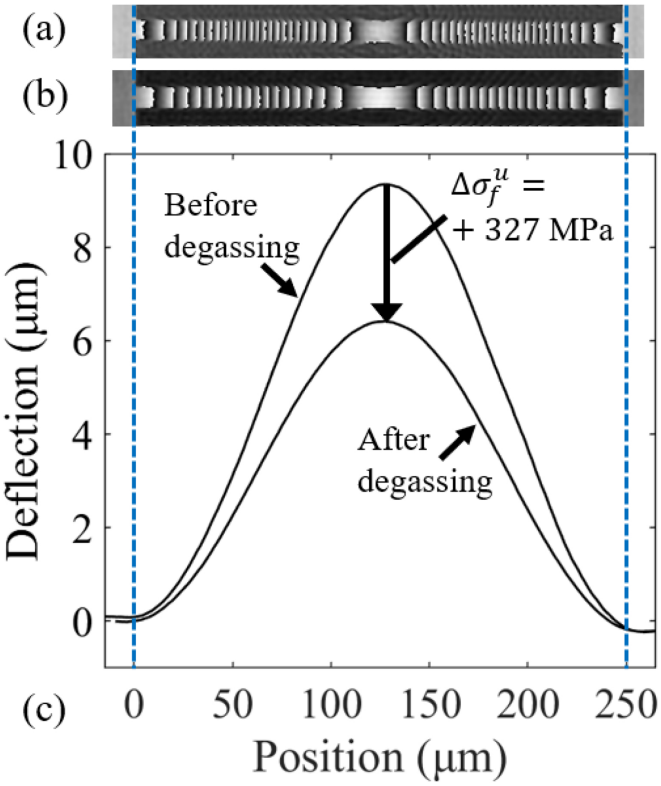

Figure 7. Fixed–fixed α-Ta beam interferograms (a) after 1 h BHF release, (b) after high temperature degassing and (c) the associated deflection curves.

4. Conclusions

This work demonstrates that the stress shift of β-Ta films towards compression after a release step by BHF arises from hydrogen injection. The hydrogen can be degassed at 500 °C in an UHV environment. By using α-Ta films to exclude the phase transition effect, it is proved that the hydrogen effect is largely reversible and the residual stress is substantially recovered by degassing. The evidence provided supports the following conclusions:

- While RIE has little or no effect on the residual stress of thick Ta films, BHF release increases the compressive stress and results in buckling of originally tensile-stressed Ta fixed–fixed beams (figure 2).
- For both blanket Ta films and fixed–fixed beams, the increase in compressive stress is linear with BHF exposure times; the biaxial stress changes are up to −490 MPa and −1 GPa after a 2.5 h exposure, respectively. fixed–fixed beams experience a doubling in the stress change compared to blanket films because the exposed area is approximately doubled (figure 3). An increase in the lattice constant of blanket Ta films further indicates the presence of injected hydrogen atoms in the Ta crystal lattices (figures 4 and 5).
- H_2 desorption starts at 400 °C, peaks around 500 °C and becomes negligible at 570 °C. Hydrogen desorption during the second thermal cycle is minimal. The maximum H_2 desorption rate for the specimen not exposed to BHF is more than 300 times less while its integrated total amount of desorption is only 1.4% of the BHF-treated specimen (figure 6).
- β-Ta films partially transform to α-Ta after annealing at 500 °C for 20 min. A 10 nm Cr seed layer nucleates the BCC α-Ta. The biaxial stress change of α-Ta is more sensitive to hydrogen incorporation compared to β-Ta and can be substantially recovered after degassing (figure 3).

The understanding gained in this work represents a useful step potentially leading to the more widespread use of Ta as a MEMS structural material in applications such as those mentioned in the Introduction [1, 2, 5, 6].

Acknowledgments

This work was partially supported by US National Science Foundation (NSF) Grant No. CMMI-1635332. We also

acknowledge the Kavcic-Moura Endowment Fund for support and use of the Materials Characterization Facility at Carnegie Mellon University under Grant No. MCF-677785.

ORCID iDs

Andrew J Gellman https://orcid.org/0000-0001-6618-7427
Maarten P De Boer https://orcid.org/0000-0003-1574-9324

References

[1] Latif R, Mastropaolo E, Bunting A, Cheung R, Koickal T, Hamilton A, Newton M and Smith L 2011 Low frequency tantalum electromechanical systems for biomimetical applications *J. Vac. Sci. Technol.* B **29** 6–11
[2] Sedky S, Fiorini P, Witvrouw A and Baert K 2019 Sputtered tantalum as a structural material for surface micromachined RF switches *Mat. Res. Soc. Symp. Proc.* **729** U3.3
[3] Touloukian Y S and Ho C Y 1975 Thermophysical Properties of Matter *Thermal Expansion of Metallic Elements and Alloys* (Lafayette, IN: Thermophysical and Electronic Properties Information Analysis Center) vol 12
[4] Okada Y and Tokumaru Y 1984 Precise determination of lattice parameter and thermal expansion coefficient of silicon between 300 and 1500 K *J. Appl. Phys.* **56** 314
[5] Steiner H, Keplinger F, Schalko J, Hortschitz W and Stifter M 2015 Highly efficient passive thermal micro-actuator *J. Microelectromech. Syst.* **24** 1981–8
[6] Mastropaolo E, Latif R, Grady E and Cheung R 2013 Control of stress in tantalum thin films for the fabrication of 3D MEMS structures *J. Vac. Sci. Technol.* B **31** 6–8
[7] Thornton J A 1977 High rate thick film growth *Ann. Rev. Mater. Sci.* **7** 239–60
[8] Doerner M F and Nix W D 1988 Stresses and deformation processes in thin films on substrates *Crit. Rev. Solid State Mater. Sci.* **14** 225–68
[9] Freund L B and Suresh S 2004 *Thin Film Materials: stress, Defect Formation and Surface Evolution* (Cambridge: Cambridge University Press)
[10] Chason E 2012 A kinetic analysis of residual stress evolution in polycrystalline thin films *Thin Solid Films* **526** 1–14
[11] Al-masha'al A, Mastropaolo E, Dunare B A, C and Cheung R 2016 Fabrication and characterisation of suspended microstructures of tantalum *J. Micromech. Microeng.* **27** 015020
[12] Wipf H 2001 Solubility and diffusion of hydrogen in pure metals and alloys *Phys. Scr.* **2001** 43–51
[13] Ferrin P, Kandoi S, Nilekar A U and Mavrikakis M 2012 Hydrogen adsorption, absorption and diffusion on and in transition metal surfaces: a DFT study *Surf. Sci.* **606** 679–89
[14] Dornheim M, Pundt A, Kirchheim R, Molen S J V D, Kooij E S, Kerssemakers J, Griessen R, Harms H and Geyer U 2003 Stress development in thin yttrium films on hard substrates during hydrogen loading *J. Appl. Phys.* **93** 8958
[15] Laudahn U, Pundt A, Bicker M, Hülsen U V, Geyer U, Wagner T and Kirchheim R 1999 Hydrogen-induced stress in Nb single layers *J. Alloys Compd.* **293** 490–4
[16] Yang Q M, Schmitz G, Fähler S, Krebs H U and Kirchheim R 1996 Hydrogen in Pd/Nb multilayers *Phys. Rev.* B **54** 9131–40
[17] Pfeiffer H and Peisl H 1977 Lattice expansion of niobium and tantalum due to dissolved hydrogen and deuterium *Phys. Lett.* A **60** 363–4
[18] Andersson G, Rgvin B, Rvarsson H and Zabel H 1997 Hydrogen-induced lattice expansion of vanadium in a Fe/V (001) single-crystal superlattice *Phys. Rev.* B **55** 905–11 (accessed 9 February 2019)
[19] Pryde J A and Tsong I T 1971 A theory of the resistivity of high-concentration interstitial alloys with application to the tantalum-hydrogen and tantalum-deuterium systems *Acta Metall.* **19** 1333–8
[20] Katz Y, Tymiak N and Gerberich W W 2001 Nanomechanical probes as new approaches to hydrogen/deformation interaction studies *Eng. Fract. Mech.* **68** 619–46
[21] Kuznetsov A S, Gleeson M A and Bijkerk F 2012 Hydrogen-induced blistering mechanisms in thin film coatings *J. Phys. Condens. Matter* **24**
[22] Čížek J *et al* 2008 Hydrogen-induced buckling of Pd films studied by positron annihilation *Appl. Surf. Sci.* **255** 241–4
[23] Eren B, Marot L, Günzburger G, Renault P O, Glatzel T, Steiner R and Meyer E 2014 Hydrogen-induced buckling of gold films *J. Phys. D Appl. Phys.* **47**
[24] Owen C V and Scott T E 1972 Relation between hydrogen embrittlement and the formation of hydride in the group v transition metals *Metall. Trans.* **3** 1717–26
[25] Pundt A, Laundahn U, Htilsen U V, Geyer U, Getzlaff M, Bode M, Wiesendanger R and Kirchheim R 2019 Hydrogen induced plastic deformation of thin films *Mater. Res. Soc. Symp. Proc.* **594** 75–86
[26] Pick M, Greene M and Strongin M 1980 Uptake rates for hydrogen by niobium and tantalum: effect of thin metallic overlayers, J *Less Common Met.* **73** 89–95
[27] Stoney G G 1909 the tension of metallic films deposited by electrolysis *Proc. R. Soc. A Math. Phys. Eng. Sci.* **82** 172–5
[28] Oliver W C and Pharr G M 1992 An improved technique for determining hardness and elastic-modulus using load and displacement sensing indentation experiments *J. Mater. Res.* **7** 1564–83
[29] Masters N D, de Boer M P, Jensen B D, Baker M S, Koester D and Boer D 2001 Side-by-side comparison of passive MEMS strain test structures under residual compression *Mech. Prop. Struct. Film. ASTM Int.*
[30] Guckel H, Randazzo T and Burns D W 1985 A simple technique for the determination of mechanical strain in thin films with applications to polysilicon *J. Appl. Phys.* **57** 1671
[31] Windischmann H 1992 Intrinsic stress in sputter-deposited thin films *Crit. Rev. Solid State Mater. Sci.* **17** 547–96
[32] Al-Masha'al A, Bunting A and Cheung R 2016 Evaluation of residual stress in sputtered tantalum thin-film *Appl. Surf. Sci.* **371** 571–5
[33] Williams K R, Gupta K, Wasilik M, Si P and Si P 2003 Etch rates for micromachining processing II *J. Microelectromech. Syst.* **12** 761–78
[34] Pick M A, Greene M G and Strongin M 1980 Uptake rates for hydrogen By niobium and tantalum: effect of thin metallic overlayers *J. Less-Common Met.* **73** 89–95
[35] Wiswall R 1978 Hydrogen storage in metals *Hydrog. Met. II* **29** 201–42
[36] Buxbaum R E and Marker T L 1993 Hydrogen transport through non-porous membranes of palladium-coated niobium, tantalum and vanadium *J. Membr. Sci.* **85** 29–38
[37] Schaumann G, Völkl J and Alefeld G 1970 The diffusion coefficients of hydrogen and deuterium in vanadium, niobium, and tantalum by Gorsky-effect measurements *Phys. Status Solidi* **42** 401–13
[38] Borgucci M V and Verdini L 1965 Electrical resistance measurements on hydrogen-charged tantalum and niobium *Phys. Status Solidi* **9** 243–50
[39] Pundt A, Nikitin E, Pekarski P and Kirchheim R 2004 Adhesion energy between metal films and polymers

obtained by studying buckling induced by hydrogen *Acta Mater.* **52** 1579–87
[40] Hirakata H, Yamada T, Nobuhara Y, Yonezu A and Minoshima K 2010 Hydrogen effect on fracture toughness of thin film/substrate interfaces *Eng. Fract. Mech.* **77** 803–18
[41] Ni L, Pocratsky R M and de Boer M P 2020 Origins of thin film delamination induced by electrodeposition and processing methods to overcome it *Thin Solid Films* **697** 137796
[42] Zhang M, Zhang Y F, Rack P D, Miller M K and Nieh T G 2007 Nanocrystalline tetragonal tantalum thin films *Scr. Mater.* **57** 1032–5
[43] Ellis E A I, Chmielus M and Baker S P 2018 Effect of sputter pressure on Ta thin films: beta phase formation, texture, and stresses *Acta Mater.* **150** 317–26
[44] Zhou Y M, Xie Z, Ma Y Z, Xia F J and Feng S L 2012 Growth and characterization of Ta/Ti bi-layer films on glass and Si (1 1 1) substrates by direct current magnetron sputtering *Appl. Surf. Sci.* **258** 7314–21
[45] Pundt A and Kirchheim R 2006 Hydrogen in metals: microstructural aspects *Annu. Rev. Mater. Res.* **36** 555–608
[46] Cabral C, Clevenger L A and Schad R G 1994 Repeated compressive stress increase with 400 °C thermal cycling in tantalum thin films due to increases in the oxygen content *J. Vac. Sci. Technol. B Microelectron. Nanom. Struct. Process.* **12** 2818
[47] Clevenger L A, Mutscheller A, Harper J M E, Cabral C and Barmak K 1992 The relationship between deposition conditions, the beta to alpha phase transformation, and stress relaxation in tantalum thin films *J. Appl. Phys.* **72** 4918–24
[48] Knepper R, Stevens B and Baker S P 2006 Effect of oxygen on the thermomechanical behavior of tantalum thin films during the B-α phase transformation *J. Appl. Phys.* **100** 123508
[49] Face D W and Prober D E 1987 Nucleation of body-centered-cubic tantalum films with a thin niobium underlayer *J. Vac. Sci. Technol. A Vac. Surf. Films* **5** 3408–11
[50] Ikeda M, Murooka M and Suzuki K 2002 Semi-epitaxial bcc Ta Growth on Metal Nitride *Jpn. J. Appl. Phys.* **41** 3902–8
[51] Ikeda M, Dohjo M and Oana Y 1989 Low resistivity quasi-epitaxial Mo-Ta alloy and high-quality anodic oxide for *a*-Si thin-film transistor liquid-crystal display *J. Appl. Phys.* **66** 2052–5
[52] Giber J and Oechsner H 1985 Dissolution of anodic Ta2O5 layers into polycrystalline tantalum *Thin Solid Films* **131** 279–87
[53] Howe R T 1988 Surface micromachining for microsensors and microactuators *Cit. J. Vac. Sci. Technol. B Microelectron. Process. Phenom.* **6** 1809